TWENTY FIRST EUROPEAN ROTORCRAFT FORUM

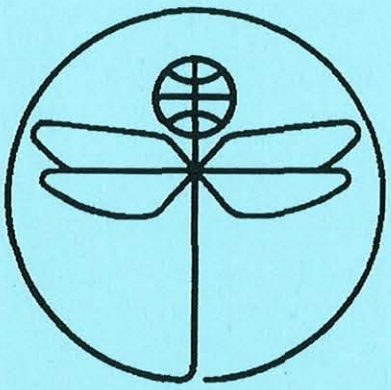

Paper No II.4

RECENT DEVELOPMENTS ON A BEM FOR AERODYNAMICS AND AEROACOUSTICS OF ROTORS

BY

M.Gennaretti, U. Iemma, L. Morino

Terza Universita di Roma, Dipartimento di Meccanica e Automatica
Rome, Italy

August 30 - September 1, 1995
SAINT - PETERSBURG, RUSSIA

Paper nr.: II.4

Recent Developments on a BEM for Aerodynamics and Aeroacoustics of Rotors.

M. Gennaretti; U. Iemma; L. Morino

TWENTY FIRST EUROPEAN ROTORCRAFT FORUM
August 30 - September 1, 1995 Saint-Petersburg, Russia

RECENT DEVELOPMENTS ON A BEM FOR AERODYNAMICS AND AEROACOUSTICS OF ROTORS

M. Gennaretti*, U. Iemma†, and L. Morino‡
* Research Associate
† Postdoctoral Fellow
‡ Professor

Terza Università degli Studi di Roma
Dipartimento di Meccanica e Automatica
via C. Segre n. 60, 00146 Rome, Italy

ABSTRACT

A general boundary integral formulation for the transonic aerodynamic and aeroacoustic analyses of lifting bodies in arbitrary motion is presented. Emphasis is given here on the analysis of the contribution of the wake and of the non-linear field terms appearing in the boundary integral representation for the velocity potential.

Numerical results obtained from the formulation outlined include both aerodynamics and aeroacoustics of helicopter rotors in hover and forward flight in subsonic flows. They are compared with both existing numerical results and experimental data. Transonic results are presented for steady flows around both fixed-wing and hovering rotors

1. INTRODUCTION

The scope of this work is to give an overview on recent developments on the aerodynamic and aeroacoustic analyses of lifting bodies in arbitrary motion, using a boundary integral formulation in terms of the velocity potential. The solution for the velocity potential is given in terms of a direct boundary integral representation extended over the body and wake surfaces. In the case of transonic flows a field integral over the portion of the fluid field where non–linear terms are not negligible is also included (*e.g.*, blade tips for helicopter rotors).

Historical review is beyond the scope of the present work; interested reader is addressed to Morino[1], and Gennaretti, Iemma, Luceri, and Morino[2].

Here, we adopt a unified aerodynamic/aeroacoustic approach valid for bodies in arbitrary rigid motion first introduced in Morino, Gennaretti, Petrocchi [3], and Gennaretti [4]. The extension of the method to the transonic analysis is based on the full-potential formulation presented in Morino and Iemma [5], and Iemma [6], which is an extension to the full-potential model of the TSP formulation of Tseng and Morino [7]. The methodologies of Morino, Gennaretti, Petrocchi [3] and Iemma [6] are combined in order to produce what we believe to be the first direct boundary-integral formulation for transonic flows in forward flight, with field sources limited to non-linear terms.

This paper is divided in five Sections. In the next Section the differential formulation for full-potential flows is presented, whereas in Section 3 we derive the boundary integral formulation for a lifting body in transonic arbitrary motion, with particular emphasis on wake and field contributions. Numerical results on aerodynamics of fixed-wings, as well as aerodynamics and aeroacoustics of hovering and advancing helicopter rotors will be shown

in Section 4. Concluding remarks are presented in Section 5. The theoretical formulation has been jointly developed by Gennaretti, Iemma and Morino. Gennaretti and Iemma were responsible for the development of the numerical algorithm, for forward flight and transonic flows, respectively.

2. FULL-POTENTIAL FLOW FORMULATION

An initially isentropic, initially irrotational flow of an inviscid, non-conducting fluid remains *isentropic and irrotational at all times*. Under these assumptions the velocity field may be expressed in terms of a scalar potential ϕ such that $\mathbf{v} = \nabla\phi$, where $\mathbf{v}$ is the fluid velocity. Then, the equations governing the problem are the continuity equation $\dot{\rho} + \nabla \cdot (\rho \mathbf{v}) = 0$, the Bernoulli theorem $\dot{\phi} + v^2/2 + h = h_\infty$ (where ρ is the air density and h is the enthalpy), and the isentropic law for ideal gases $h/\rho^{\gamma-1} =$ constant. Combining the above equations, considering that $h = \gamma p/(\gamma - 1)\rho$, and moving all the non-linear terms to the right hand side of the equation, one obtains, in a frame of reference fixed with the undisturbed flow (air frame of reference), the following form for the non-linear equation of the velocity potential

$$\nabla^2\phi - \frac{1}{a_\infty^2}\frac{\partial^2\phi}{\partial t^2} = \sigma \tag{1}$$

where $a_\infty^2 = \gamma p_\infty/\rho_\infty$ is the speed of sound in the undisturbed flow, whereas σ denotes all the non-linear terms. The full-potential conservative form for σ is given by (see [8]):

$$\sigma = \nabla \cdot \left[\left(1 - \frac{\rho}{\rho_\infty}\right)\nabla\phi\right] - \frac{\partial}{\partial t}\left(\frac{\rho}{\rho_\infty} + \frac{1}{a_\infty^2}\frac{\partial\phi}{\partial t}\right) = \nabla \cdot \tilde{\mathbf{b}} + \frac{\partial \hat{b}}{\partial t} \tag{2}$$

where ρ is obtained from the Bernoulli theorem

$$\frac{\rho}{\rho_\infty} = \left[1 - \frac{1}{h_\infty}(\dot{\phi} + \frac{v^2}{2})\right]^{\frac{1}{\gamma-1}}. \tag{3}$$

The differential formulation for potential flows is completed by the boundary conditions. The body surface $\mathcal{S}_B$ is assumed to be impermeable. This yields $(\mathbf{v} - \mathbf{v}_B) \cdot \mathbf{n} = 0$, where $\mathbf{v}_B$ represents the velocity of a body surface point and $\mathbf{n}$ is the unit normal to such a surface. Furthermore, in the air frame of reference we have $\mathbf{v} = 0$ at infinity. In terms of the velocity potential, we obtain $\partial\phi/\partial n = \mathbf{v}_B \cdot \mathbf{n}$ for $\mathbf{x} \in \mathcal{S}_B$, where $\mathcal{S}_B$ represents the body surface, and $\phi = 0$ at infinity. In addition, we need a boundary condition on the wake (see [8] for further details). The wake is a surface of discontinuity for the velocity potential. From principles of conservation of mass and momentum one obtains both that the wake surface $\mathcal{S}_W$ cannot be crossed by fluid particles ($\mathbf{v} \cdot \mathbf{n} = \mathbf{v}_W \cdot \mathbf{n}$, where $\mathbf{v}_W$ is the velocity of points on $\mathcal{S}_W$) and that pressure is continuous across it. Again, in terms of the velocity potential, the first condition yields (see [8]) $\Delta(\partial\phi/\partial n) = 0$ whereas the second one, using Bernoulli's theorem, yields $D_W(\Delta\phi)/Dt = 0$ where $D_W/Dt = \partial/\partial t + \mathbf{v}_W \cdot \nabla$, with $\mathbf{v}_W$ representing the velocity of a point $\mathbf{x}_W$ of the wake (*i.e.*, the average of the velocity on the two sides of the wake). This condition states that $\Delta\phi$ is constant in time following a wake point and equal to the value it had when $\mathbf{x}_W$ left the trailing edge. This value is obtained from $\Delta\phi$ on the body, in correspondence of the trailing edge (trailing-edge condition).

3. BOUNDARY INTEGRAL FORMULATION

In this section we will present the boundary integral formulation for the solution of the non-linear wave equation. Since the emphasis of the present work is on the applications of

the method, we will not enter into mathematical details. This are extensively addressed in [2].

Consider two disjoint closed rigid surfaces $\mathcal{S}_1$ and $\mathcal{S}_2$ surrounding, respectively, the volume $\mathcal{D}_1$ occupied by the body and the volume $\mathcal{D}_2$ occupied by a thin fluid region containing the wake surface (assumed to be undeformed, see later). It can be shown that the integral representation for the wave equation, Eq. 1, has the form

$$E(\xi_*,\tau_*)\phi(\xi_*,\tau_*) = \mathcal{I}_1 + \mathcal{I}_2 + \iiiint_{-\infty}^{\infty} G\,E\,\sigma\,d\mathcal{V}d\tau \tag{4}$$

where (ξ,τ) is an event in the space connected with the undisturbed air, E is a domain function $E(\xi,\tau)$ (defined as $E=1$ in $\mathcal{V}$, where $\mathcal{V}$ denotes the fluid region, and $E=0$ otherwise), and $\mathcal{I}_i$ is the integral contribution of the i-th surface, which can be written in the general form

$$\begin{aligned}\mathcal{I}_i(\xi_*,\tau_*) &= \oiint_{\mathcal{S}_i}\left[\frac{\partial\phi}{\partial\tilde{n}}G_0 - \phi\frac{\partial G_0}{\partial\tilde{n}}\right]_{t=t_*-\theta} d\mathcal{S} \\ &+ \oiint_{\mathcal{S}_i}\left[G_0\frac{\partial\phi}{\partial t}\left(\frac{\partial\theta}{\partial\tilde{n}} + 2\frac{\mathrm{v}_x\cdot\mathrm{n}}{a_\infty^2}\right)\right]_{t=t_*-\theta} d\mathcal{S} \\ &+ \frac{1}{a_\infty^2}\oiint_{\mathcal{S}_i}\left[\phi\,G_0\frac{\partial}{\partial t}[\mathrm{v}_x\cdot\mathrm{n}(1-\mathrm{v}_x\cdot\nabla\theta)]\right]_{t=t_*-\theta} d\mathcal{S}\end{aligned} \tag{5}$$

where $\partial/\partial\tilde{n} = \partial/\partial n - \mathrm{v}_x\cdot\mathrm{n}\;\mathrm{v}_x\cdot\nabla/a_\infty^2$, and v_x represents the velocity of a point x of the body space with respect to the air space (written in the body space).

Equation 4, with $\mathcal{I}_i$ expressed by Eq. 5 is the boundary integral representation for the solution to Eq. 1 with the initial conditions and infinity boundary conditions defined above. If ξ_* tends to the boundary, Eq. 4 yields a compatibility condition that must be satisfied by the solution of the problem. In our case $\partial\phi/\partial n$ is known from the boundary conditions of impermeability of the body surface, and therefore such compatibility condition is an integral equation for ϕ on the boundary. Once ϕ on the surface is known, ϕ and hence v may be evaluated anywhere in the field. Then, the pressure (and hence, the acoustic noise) may be computed using the Bernoulli theorem.

3.1 Body contribution

First, we consider the body contribution. For the case of interest in the present paper, *i.e.*, a helicopter rotor in forward flight, it is a straightforward application of Eq. 5 with

$$\mathrm{v}_x(\mathrm{x},t) = \mathrm{R}^{-1}\mathrm{v}_0 + \omega\times\mathrm{x} \tag{6}$$

where v_0 is the air-space vector of the velocity of the point $\mathrm{x}=0$ and ω is the angular velocity of the rotor, both with respect to the air frame of reference.

3.2 Wake contribution

For the sake of clarity, let us limit the discussion to the case of a single wake (even if multiple wake configurations may be similarly treated). In addition, we assume that the motion of the wake surface with respect to the air frame of reference is negligible.[1] In this case, it is possible to obtain the contribution of the wake by evaluating that from surface $\mathcal{S}_2$

[1] This is typically true for airplanes in maneuvering and helicopter rotors in forward flight. If this is not true, the formulation may be extended using the formulation for surfaces that move in arbitrary (not rigid-body) motion (see [4]).

tending to the wake surface (*i.e.*, by taking the limit of $\mathcal{I}_2$ for the thickness of $\mathcal{D}_2$ tending to zero). The final form of the wake contribution is

$$\begin{aligned} \mathcal{I}_W(\xi_*, \tau_*) &= -\iint_{\hat{\mathcal{S}}_W} \Delta\hat{\phi}\, \frac{\partial G_0}{\partial n}\, d\mathcal{S} \\ &+ \int_{\lambda_1}^{\lambda_2} \left[\Delta\hat{\phi}\, G_0\, \frac{1}{1+M_\varrho}\, \frac{\partial \varrho}{\partial n}\, \frac{v_\nu}{a_\infty} \right]_{\alpha=\alpha_0} d\lambda \end{aligned} \tag{7}$$

where $1 + M_\varrho = 1 + (\varrho \cdot \mathrm{v}_{TE})/(a_\infty \varrho) > 0$, and $1 + M_\varrho$ is known as the Doppler factor. In the previous equation, λ and α identify a system of curvilinear coordinates over the surface of the wake. In particular, λ represents the arclength along the trailing edge, and α identifies the trailing edge location at a certain time. The last integral is evaluated for $\alpha = \alpha_0$, *i.e.*, along the line $\hat{\mathcal{L}}_W$ which separates the influencing portion of the wake $\hat{\mathcal{S}}_W$ from the non-influencing one.

3.3 Field contribution

Finally, in the case of transonic flow configuration the contribution from the field term in Eq. 4 cannot be neglected. In order to evaluate such contribution, let us note that the non-linear term σ becomes relevant only in a limited fluid region $\mathcal{V}_\sigma$ around the body surface. In the case of interest here, such region is that at the tip of the rotor blades. Hence, for the sake of simplicity, it is worth to evaluate the field-term contribution in the body frame of reference, where $\mathcal{V}_\sigma$ is fixed. In this case, the non-linear term contribution is expressed as

$$\mathcal{I}_V = \iiint_{\mathcal{V}_\sigma} [G_0\, \sigma]_{t=t_*-\theta}\, d\mathcal{V} \tag{8}$$

where $\sigma = \nabla \cdot \mathrm{b} + \partial \hat{b}/\partial t$ with $\mathrm{b} = \tilde{\mathrm{b}} - \hat{b}\, \mathrm{v}_x$ (note that here the time derivative is evaluated in the body frame of reference, whereas in Eq. 2 was understood in the air frame of reference).

4. NUMERICAL APPLICATIONS

The formulation presented has been applied to the aerodynamic and aeroacoustic analysis of rotors in several flight conditions. In particular, validation in the subsonic regime has been performed for both hover and forward flight conditions, whereas in the transonic range the analysis has been limited, thus for, to hovering rotors. For the sake of completeness, we include here also some results obtained recently concerning two- and three-dimensional transonic analysis of bodies in uniform translation. The validation of the present formulation for transonic rotors in forward flight is now under way for the limited case of non-lifting rotors.

4.1 Subsonic hovering rotors

For the subsonic hovering rotor analysis, we have considered a configuration studied in [9] at the DNW for the experimental program within the HELINOISE project. In that experimental program, the rotor tested was a 40%-geometrically and dynamically scaled model of a four-bladed, hingless BO-105 main rotor. The rotor had a diameter of 4m with a root cut-out of 0.35m and a chord lenght of 0.121m. The blades had a $-8°$ of linear twist, with a modified NACA 23012 profile, and a coning angle of 2.5°. The nominal rotor operational speed was 1040rpm. For the hovering configuration the tip Mach number was $M_{TIP} = 0.645$. We have considered two observer locations for the evaluation of the acoustic signal: the first is at the distance of 4.826m from the rotor hub, the second one is at a distance of 4m from the

rotor hub, both placed 2.3m below the rotor disk (microphone 11 and microphone 6 in [9], respectively). Figures 1 and 2 depict, for the two observer locations, the comparison of the measured acoustic signal with the two acoustic signatures obtained by using two different wake geometries (the first named 'Landgrebe' is based on the wake model determined in [10], and is much closer to the actual shape of a hovering rotor wake than the second one, an helicoidal-shaped wake). Observing these figures it is possible to note the capability of the formulation to capture with good approximation the noise disturbance generated by the rotor, as well as the importance of the wake geometry adopted in the potential formulation. Indeed, in the case of hovering rotors, the wake generated remains in the vicinity of the rotor, therefore having a strong effect on the aerodynamic field around the blades.

4.2 Subsonic advancing rotors

Also for the case of rotors in forward flight, we have analysed a test case studied in [9] and a test case studied in [11].

The test case studied in [9] is that of a BO-105 rotor in ascent flight, with an effective tip path plane angle $\alpha'_{TPP} = -14.63°$, advance ratio $\mu = 0.148$, hovering tip Mach number $M_{TIP} = 0.645$, and feathering motion. In Fig. 3 we show the comparison between the measured acoustic signal and the computed one, for an observer placed 2.3m below the rotor disk, at a distance of 3.36m from the rotor hub (microphone 1 in [9]). The agreement between the two results is satisfactory, even with a numerical analysis performed using a simple wake geometry (obtained as the surface swept by the blade trailing edges during their motions). Such a result is not surprising, since for rotors in forward flight the wake rapidly moves away from the blade, and only a limited portion of its surface strongly affects the blade aerodynamics. Hence, even the simple wake geometry used in this case simulates with satisfactory approximation the aerodynamic effects induced by the actual one. This is confirmed by the comparison of the pressure distribution predicted by the present method with the experimental results of [9]. This is presented in Figs. 4 to 11 for several locations along the blade. Specifically, Figs. 4, 5, 6 and 7 correspond to the blade section at $r/R = 0.75$ for four different values of the azimuthal angle (0°, 90°, 120°, 270°, respectively), whereas Figs. 8, 9, 10 and 11 are related to the section at $r/R = 0.97$ (for the same azimuthal positions).

Then, we consider the forward flight case studied in [11]. It consists of the articulated UH-1H rotor with an angle of attack of the rotor shaft $\alpha_F = -8°$, advance ratio $\mu = 0.124$, and both flapping and feathering motions. Figure 12 depicts the comparison between the acoustic-pressure time history computed in [11] and that obtained by the present formulation. The two numerical results appear to be in a good agreement, confirming the capability of the presented formulation to capture the aerodynamic/aeroacoustic solution for rotors in forward flight.

4.3 Transonics

Next, we present some results concerning transonic flows. For the sake of completeness, validations for steady two-dimensional supercritical flows are presented first, in order to emphasize the good level of accuracy reached with respect to other CFD methods. Figure 13 presents the pressure distribution on a circular cylinder at $M_\infty = 0.5$. In this flow configuration a strong shock wave occurs (the local Mach number approaches 3 in the supersonic region). Thus, we are beyond the applicability of the potential model, since the vorticity generated by the discontinuity is not negligible. The test case is important to verify the behavior of the method in presence of strong shocks. The comparison of the integral solution for two different mesh sizes with the finite volume solution, obtained by Salas [12] using a Jameson

scheme[13], shows a satisfactory agreement in terms of shock position and resolution. Furthermore, the iterative process for the evaluation of the non-linear terms converges very fast, despite the presence of a strong discontinuity, as can be seen in Fig. 14. The same level of accuracy is verified in Fig. 15, where the flow about a NACA 0012 airfoil at $M_\infty = 0.82$ and $\alpha = 0°$ is analyzed. The pressure distribution is compared with full-potential finite-volume results obtained using a Jameson scheme [13]. The result obtained by BEM with a C-type grid using 70×20 volume elements is in good agreement with the finite-volume one, even if a low number of elements is employed. The use of a C-type grid, rather than the more crude H geometry, introduce a major improvement in terms of the stability of the iterative process (see [2]). This is confirmed in three-dimensional analysis. In fact, the C-type grid allows the analysis of those wing geometries for which the H-type mesh fails. Figure 16 shows the pressure distribution for swept, tapered wing ($\Lambda = 10°$, tap. ratio = 1.7) at $M_\infty = 0.85$. The pressure coefficient presents a regular behaviour in the spanwise direction, even if the number of the sections used is small, with a good reproduction of the tip effect. The convergence of the iterative process is fast and monotone, as it may be seen in Fig. 17. In Fig. 18 the wing has a sweep angle $\Lambda = 25°$ with a taper ratio of 2.5. The Mach number is $M_\infty = 0.85$. The effect of the sweep angle is well captured by the method. The convergence behavior is good, as shown by Fig. 19. Note that, for such a configuration, the convergence was not insured when the H-type grid was used.

Next, we analyze the transonic flow around a non-lifting 1/7 scale UH-1H hovering rotor with tip Mach number $M_{TIP} = 0.88$, that is one of the test cases considered in [14]. Figure 20 shows the computed pressure distribution at the blade section $r/R = 0.89$, whereas the section $r/R = 0.95$ is presented in Fig. 21. Comparison with CFD full-potential and Euler solutions presented in [14] are included. The qualitative agreement is acceptable, but computed shock position is clearly located upwind with respect to that in the reference results. For such a configuration, our full-potential solution obtained with a H-type grid appears to be closer to the CFD Euler one rather than to the CFD full-potential one. Probably, the error is induced by the rude geometry field grid that has been employed with the H-type grid, to ensure convergence of the iteration on non-linear contributions. Therefore, the use of a C-type grid in the field appears to be necessary in order to be able to take advantage of a more refined grid geometry.

Finally, a transonic acoustic result obtained with the present unified aerodynamic/aeroacoustic integral formulation are presented. Again, we consider the 1/7 scale UH-1H non-lifting hovering rotor with tip Mach number $M_{TIP} = 0.85$. Figure 22 depicts the acoustic pressure computed by our methodology for an in-plane observer located at a distance $d = 3.09R$ from the rotor. For the same test case, Fig. 23 shows the numerical results obtained by a Ffowcs Williams and Hawkings formulation based on CFD aerodynamic data [15]; these results may be compared with the experimental and numerical results presented in [16] (shown in Fig. 24). All the acoustic results are in good agreement. Observe that the noise components have different meanings for the formulations. Specifically, in our case, the acoustic signal may be decomposed into a body source contribution, and a field source contribution (the body doublet contribution being negligible for non-lifting cases). On the other hand, the acoustic solution based on the Ffowcs Williams and Hawkings equation is typically decomposed into a thickness and a quadrupole noise (loading noise is not present for non-lifting cases). The relationship between the two sets of components is not a simple matter to determine, and in general they are different.

5. CONCLUDING REMARKS

A boundary integral formulation for the unified aerodynamic and aeroacoustic transonic full-potential analysis of rigid lifting bodies in arbitrary motion has been presented.

Numerical results concerning hovering and advancing rotor configurations have been presented in order to demonstrate the capability of the methodology to capture aerodynamic and aeroacoustic solutions. For subsonic flow rotors in hover and forward flight, the comparison with existing numerical results and avalaible experimental data has shown a good agreement both for the aerodynamic solution and the aeroacoustic one.

For transonic flow validation we have considered 2D non-lifting airfoils as well as non-lifting wing and hovering rotors. The 2D investigations have shown a very good agreement with existing numerical results, and have also evidenced the enhancement obtained by the use of a C-type grid.

The aeroacoustic solution for non-lifting hovering rotors appears to be in good agreement with existing numerical results (based on the solution of the Ffowcs Williams and Hawkings equation) and with experimental data. The aerodynamic solution calculated is comparable with existing CFD results, but further investigations is required in order to understand the discrepancy in the vicinity of the shock.

REFERENCES

1. Morino, L., "Boundary Integral Equations in Aerodynamics," Appl. Mech. Rev., vol. 46, no. 8, 1993.

2. Gennaretti, M., Iemma, U., Luceri, L., and Morino, L. "An Integral Method for Transonic Aerodynamics and Aeroacoustics of Rotors in Forward Flight", first joint CEAS/AIAA Aeroacoustics Conference, Munich, Germany, 1995.

3. Morino, L., Gennaretti, M., Petrocchi, P., "A General Theory of Potential Aerodynamics with Applications to Helicopter Rotor-Fuselage Interaction", IABEM Conference 91, Kyoto, Japan, 1991.

4. Gennaretti, M., "Una Formulazione Integrale di Contorno per la Trattazione Unificata di Flussi Aeronautici Viscosi e Potenziali", Tesi di Dottorato di Ricerca, Università di Roma "La Sapienza", Rome, Italy, 1993. (in Italian)

5. Morino, L. and Iemma, U., "Boundary Integral Equations and Conservative Dissipation Schemes for Full Potential Transonic Flows, Computational Mechanics", 13, pp 90-99, 1993.

6. Iemma, U., "Metodi Integrali in Aerodinamica Transonica," Tesi di Dottorato di Ricerca, Università di Roma "La Sapienza", Rome, Italy, 1994. (in Italian)

7. Tseng, K. and Morino, L., "Nonlinear Green's Function Method for Unsteady Transonic Flows", in Nixon, D. (ed), "Transonic Aerodynamics", Progress in Aeronautics and Astronautics, 81, 1982.

8. Morino, L., and Tseng, K., "A General Theory of Unsteady Compressible Potential Flows with Applications to Aeroplanes and Rotors," Eds.: P. K. Banerjee and L. Morino, Developments in Boundary Element Methods, Volume 6: Nonlinear Problems of Fluid Dynamics, Elsevier Applied Science Publishers, Barking, UK, 1990.

9. Splettstoesser, W.R., Junker, B., Schultz, K.-J., Wagner, W., Weitemeyer, W., Protopsaltis, A., and Fertis, D., "The HELINOISE Aeroacoustic Rotor Test in the DNW - Test Documentation and Representative Results," DLR-Mitt. 93-09, 1993.

10. Landgrebe, A.J., "An Analytical and Experimental Investigation of Helicopter Rotor Hover Performance and Wake Geometry Characteristics," USAAMRDL TR-71-24, U.S. Army, 1971.

11. Brentner, K.S., "Prediction of Helicopter Rotor Discrete Frequency Noise," NASA TM-87721, 1986.

12. Salas, M.D., "Recent developments in transonic Euler flow over a circular cylinder", NASA Technical Memorandum no. 83282, Langley Research Center, Hampton, Virginia, 1982.

13. Jameson, A., "Transonic Potential Flow Calculation Using Conservation Form,' AIAA 2th Computational Fluid Dynamic Conference, pp. 148-161, 1975.

14. Prieur, J., Costes, M. and Baeder, J.D., "Aerodynamic and Acoustic Calculations of Transonic Nonlifting Hovering Rotors", International Technical Specialists Meeting on Rotorcraft and Rotor Fluid Dynamics, Philadelphia, Penn., 1993.

15. *Ianniello, S. and De Bernardis*, "Calculation of High Speed Noise From Helicopter Rotors Using Different Description of Quadrupole Source", Proceedings of AGARD Symposium on Aerodynamics and Aeroacoustics of Rotorcraft, Berlin, Germany, 1994.

16. Baeder, J.D., Gallman, J.M. and Yu, Y.H., "A Computational Study of the Aeroacoustics of Rotors in Hover", American Helicopter Society 49th Annual Forum, St. Louis, Missouri, 1993.

ACKNOWLEDGEMENTS

This paper has been partially supported by the European Union under the BRITE EURAM program (project HELISHAPE) and by AGUSTA ELI S.r.l. The support of Dr. Iemma through a postdoctoral fellowship of AGUSTA is also gratefully acknowledged. The authors wish to thank Dr. Luigi Luceri for his cooperation in the numerical computations. The numerical results were obtained with the IBM RISC 6000 workstations of the Aerospace Department of the University of Roma "La Sapienza", which has kindly hosted the authors.

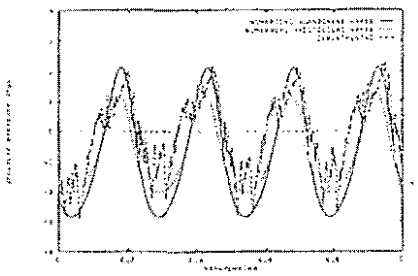

Figure 1

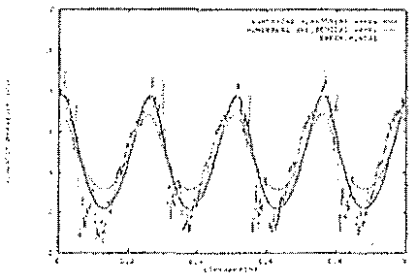

Figure 2

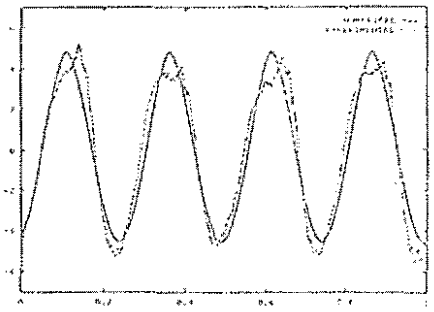

Figure 3

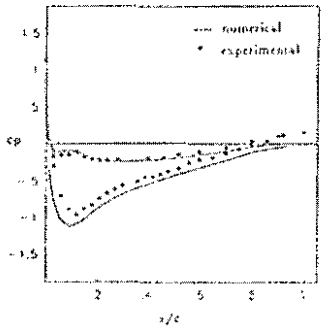

Figure 4

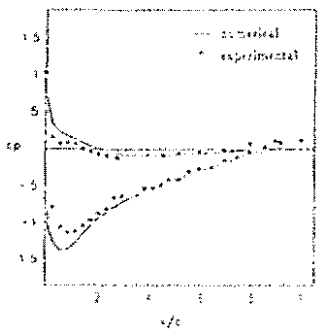

Figure 5

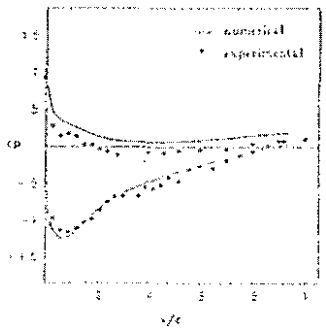

Figure 6

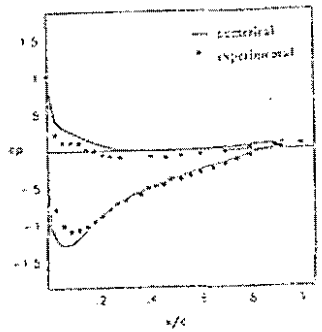

Figure 7

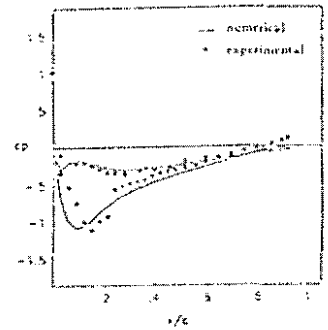

Figure 8

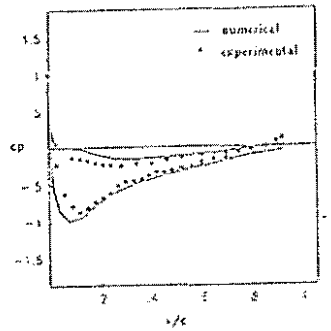

Figure 9

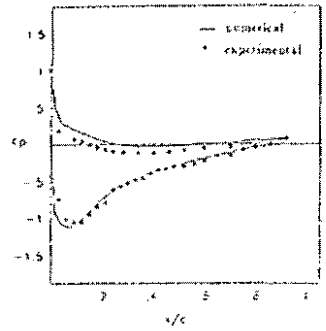

Figure 10

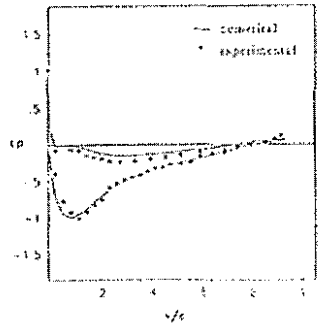

Figure 11

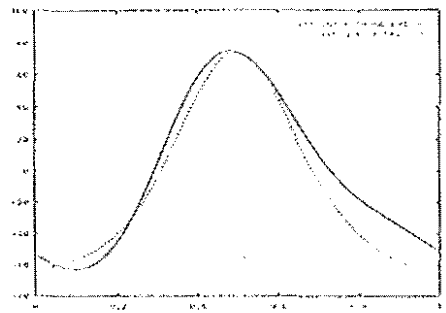

Figure 12

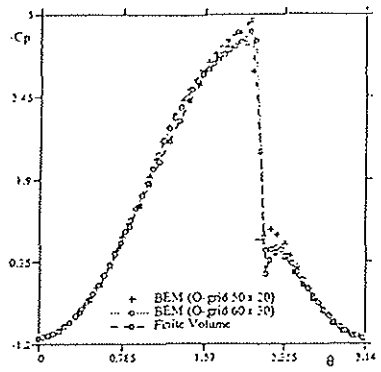

Figure 13

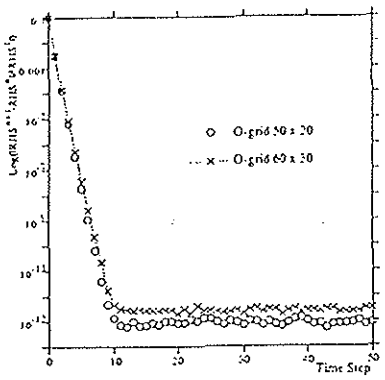

Figure 14

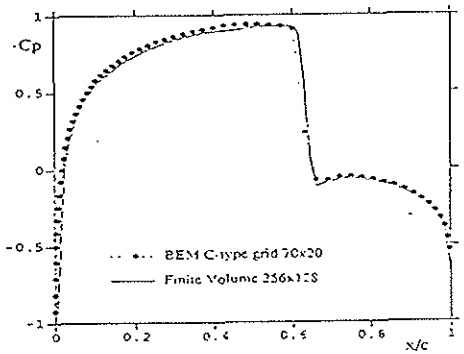

Figure 15

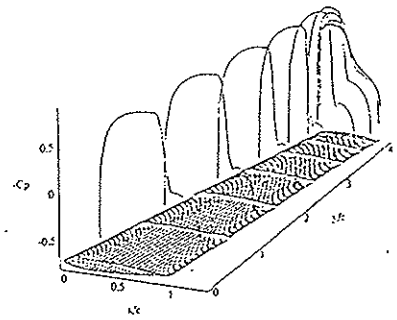

Figure 16

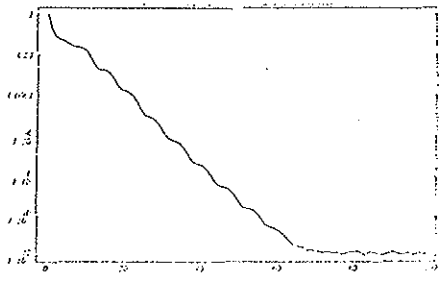

Figure 17

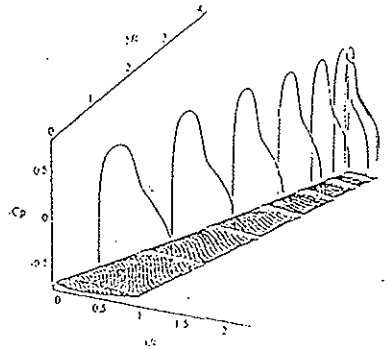

Figure 18

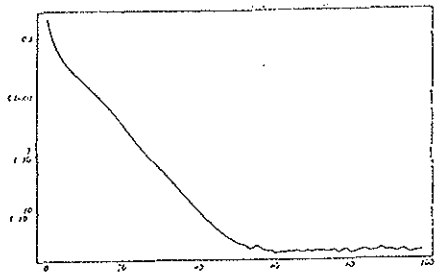

Figure 19

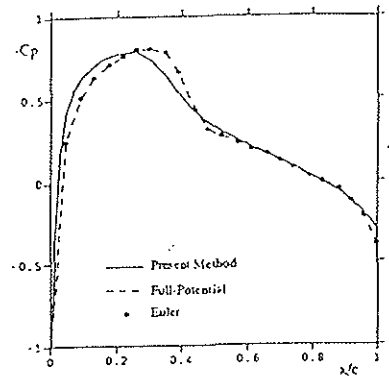

Figure 20

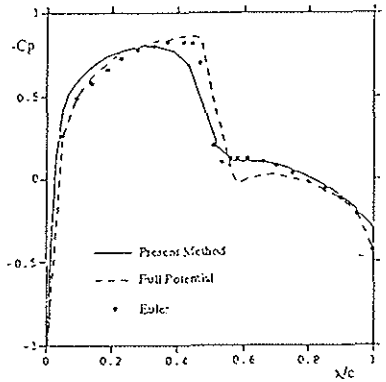

Figure 21

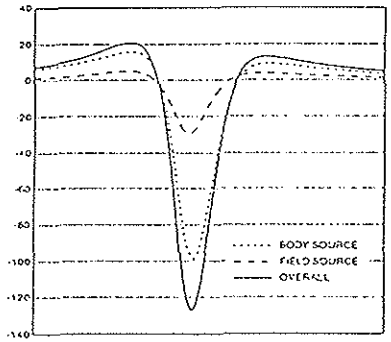

Figure 22

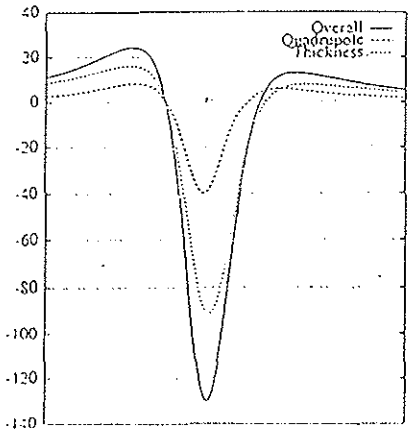

Figure 23

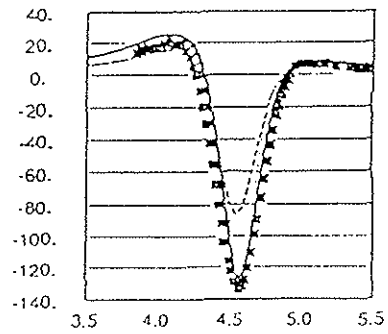

Figure 24